ACS Catalysis

Research Article

pubs.acs.org/acscatalysis

Mechanistic Investigation of Isopropanol Conversion on Alumina Catalysts: Location of Active Sites for Alkene/Ether Production

Kim Larmier,[*,†,‡,§] Céline Chizallet,[*,§] Nicolas Cadran,[§] Sylvie Maury,[§] Johnny Abboud,[†,‡] Anne-Félicie Lamic-Humblot,[†,‡] Eric Marceau,[*,†,‡] and Hélène Lauron-Pernot[†,‡]

[†]Sorbonne Universités, UPMC Univ Paris 06, UMR 7197 CNRS, Laboratoire de Réactivité de Surface, F-75005 Paris, France

[‡]CNRS, UMR 7197 CNRS, Laboratoire de Réactivité de Surface, F-75005 Paris, France

[§]IFP Energies nouvelles, Direction Catalyse et Séparation, Rond-Point de l'échangeur de Solaize, 69360 Solaize, France

Supporting Information

ABSTRACT: Alcohol dehydration is of prominent relevance in the context of biomass conversion. This reaction can be efficiently catalyzed by alumina surfaces, but the nature of active sites, the mechanisms involved, and the key parameters to tune both the activity and the alkene/ether selectivity remain a matter of debate. In the present paper, isopropanol dehydration to propene and diisopropylether over γ-alumina, δ-alumina, and sodium-poisoned γ-alumina was investigated through a combined experimental and theoretical study. The experimental kinetic study shows that dehydration occurs following the same reaction mechanism on all materials, although γ-alumina activated above 450 °C exhibits the highest density of active sites and the highest global activity. Results suggest that all the reaction pathways involved in dehydration require the same set of adjacent active sites located on the (100) facets of γ-alumina. DFT transition-state calculations of the formation of propene and diisopropylether on the main terminations of alumina, (110) and (100), were also performed. The less activated pathways for both the formation of the olefin (E2 mechanism) and the formation of the ether (S_N2 mechanism) were found on a Al_V Lewis acidic site of the (100) termination, with calculated activation enthalpies (125 and 112 kJ·mol^{-1} for propene and diisopropylether formation, respectively) in good agreement with the experimental values (128 and 118 kJ·mol^{-1}, respectively). The higher or lesser selectivity toward propene or ether appears to originate from significantly different activation entropies. The effect of coadsorbed sodium on the reaction is linked to the poisoning of Al sites by neighboring, Na-stabilized OH groups, but no influence of sodium on distant sites is evidenced. Reaction temperature is identified as the main key parameter to tune alkene/ether selectivity rather than morphology effects, which in turn affect drastically the number of available active sites, and thus catalytic activity.

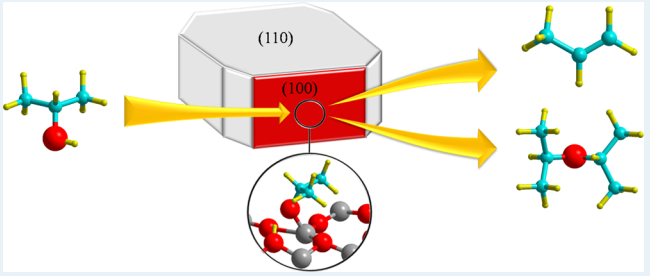

KEYWORDS: *γ-Al_2O_3, δ-Al_2O_3, sodium poisoning, isopropanol, alcohol dehydration, propene, diisopropylether, Density Functional Theory, kinetics, activation energy, entropy*

1. INTRODUCTION

The upgrading of lignocellulosic biomass by thermochemical or biochemical methods yields oxygenated species which can be successfully converted into platform chemicals or fuels through processes involving heterogeneous catalysis.[1−4] In particular, the hydrolysis of cellulose and subsequent fermentation of sugars lead to short chain alcohols: mostly ethanol,[5,6] but also *n*-propanol, isopropanol, or butanol depending on the microorganisms selected for fermentation.[7−9] Valuable alkenes and ethers are obtained by dehydration of alcohols on acidic catalysts:[10,11] in the case of isopropanol, propene, mainly employed for the synthesis of polypropylene, and diisopropylether, which is used as an additive to some fuels (Figure 1).

γ-Alumina is a cost-effective and efficient catalyst for dehydration reactions, and as a consequence, it is frequently used for application at the industrial scale. When starting from long-chain alcohols (>C_4), nearly exclusively alkenes are formed, but from short-chain alcohols, both alkenes and ethers can be obtained.[12−14] In the case of isopropanol, propene is the major product while diisopropylether is a byproduct.[12] In terms of atom economy, understanding the main factors governing

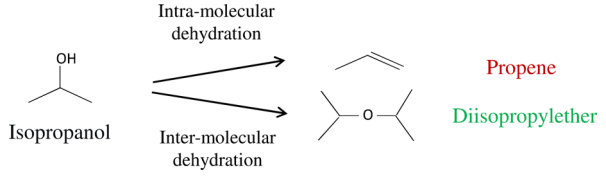

Figure 1. Dehydration pathways for isopropanol.

Received: February 17, 2015
Revised: May 29, 2015
Published: June 3, 2015

DOI: 10.1021/acscatal.5b00723
ACS Catal. 2015, 5, 4423−4437

the alkene-to-ether selectivity is of particular importance for a rational design of the catalyst.

Knoezinger et al. dedicated an extensive set of experimental studies to the dehydration of various alcohols on alumina.[12,15−24] The proposed reaction network included direct reactions (unimolecular dehydration for the alkene formation and bimolecular dehydration for ether formation, Figure 2) and

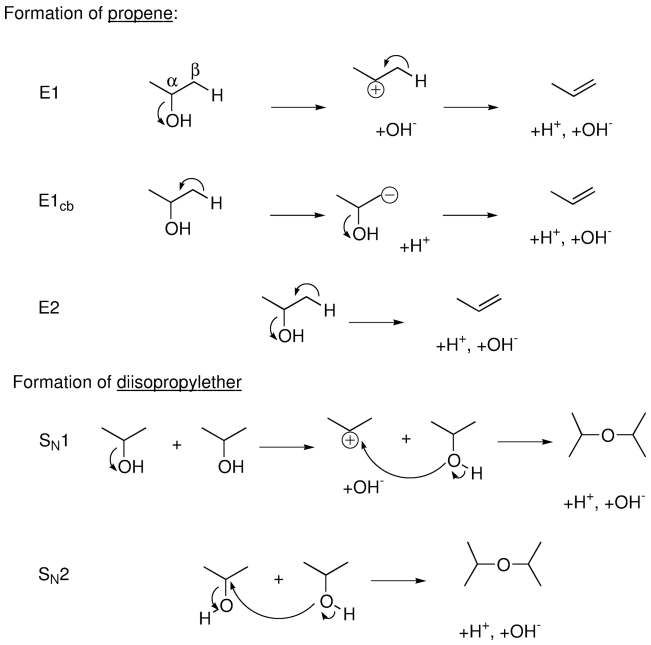

Figure 2. Schematic representation of the potential mechanisms involved in the dehydration of isopropanol. For the sake of clarity, the surface is not represented, although it can stabilize the different species. In the present paper, we will use the following naming: α for the carbon atom bearing the hydroxyl group, and β for the nearest carbon atoms, with H_β the hydrogen atoms bound to C_β.

secondary reactions such as the decomposition of ether into alkene and alcohol.[15] Several authors support the intervention of Lewis acidic sites (with alcoholate species adsorbed on Al atoms as intermediates[25−28]) and of surface basic sites, which must be strong enough to withdraw the β-hydrogen atom of the alcohol.[29] Ethers are usually considered to originate from a S_N2 mechanism (Figure 2) involving intermediates adsorbed on acidic or basic sites.[30−33] However, whether the two pathways are competitive or not in terms of active sites, and on which facets of alumina these sites are located, has seldom been investigated. Kwak et al.[28] proposed that alkene is formed on the (100) terminations of γ-Al_2O_3, but they did not consider the formation of ether. DeWilde et al.[34] proposed that ethylene and diethyl ether are formed on nonequivalent acidic sites but did not suggest a preferential facet. How the alumina selectivities to alkene and ether depend on the material morphology remains to be unraveled.

In recent years, the mechanisms of alcohol (mainly ethanol) dehydration into alkenes on γ-alumina surfaces has been investigated by computational methods, with contradictory results.[35−41] Kwak et al.[36] supported a two-step mechanism for the alkene formation, but Vlachos et al.[37−39,41] and Kostestkyy et al.[40] rather favored a concerted E2 mechanism (Figure 2). Very few studies address the formation of ether, the selectivity issue, the potential coexistence of active sites on different facets, and compare experimental and DFT results. Roy et al.,[37] Kosteskyy et al.,[40] and Kwak et al.[36] did not study the formation of ether, and DFT calculations were focused on a unique facet. Christiansen et al.[38] studied the mechanism of ethylene and diethyl ether formation on the (100) γ-Al_2O_3 surface only. Whether dehydration is oriented toward alkene or ether was derived from the relative stability of adsorbed intermediates as a function of temperature. Selectivity variations were not discussed on a quantitative basis, which is critical for the optimization of the catalyst. The other major termination, (110), was investigated by Jenness et al.[39] but without considering dispersion forces and without comparing DFT results with experimental data. Christiansen et al.[41] very recently compared DFT results with experimental measurements, but they only considered dehydrated (111) terminations.

In the present paper, we will explicitly address the alkene-to-ether selectivity issue in the case of a secondary alcohol, isopropanol. We propose to combine experimental and theoretical approaches of the reactivity of isopropanol on γ-alumina in order to compare the potential activity of surface sites for both dehydration reactions on the two major facets of alumina, (100) and (110). We endeavor to shed light on the molecular aspects of these reactions by means of *ab initio* transition state calculations, and we suggest intermediates, sites, and mechanisms that reflect the tendencies evidenced by the kinetic study.

2. EXPERIMENTAL SECTION AND METHODS

2.1. Materials. Four aluminic materials were employed in this study: a commercial γ-alumina, provided by Sasol (Puralox TH 100/150, specific surface area (S.S.A.) 145 $m^2 \cdot g^{-1}$, Na content <50 ppm), a commercial δ-alumina (provided by AXENS, S.S.A. 140 $m^2 \cdot g^{-1}$, Na content <50 ppm), and two sodium-doped γ-alumina samples. The latter ones were prepared by incipient wetness impregnation of γ-alumina with $NaNO_3$ (Sigma-Aldrich) or NaOH (Sigma-Aldrich) aqueous solutions, to achieve a 0.1 wt % sodium loading, and calcined at 650 °C for 5 h under air (5 °C·min^{-1}). To ensure better comparison of materials, the γ- and δ- alumina samples were also calcined at 650 °C for 3 h prior to any catalytic experiment. It was checked by X-ray Diffraction (XRD) that the γ- to δ-transition does not occur in these conditions (see Supporting Information, Figure S1).

Aluminas were characterized by XRD (D8 Bruker diffractometer, Bragg−Brentano geometry, Cu Kα, λ = 0.154056 nm) and by nitrogen physisorption on a Belsorp-max apparatus (BEL Japan) at liquid nitrogen temperature. The specific surface area was calculated according to the B.E.T. method. Structural and textural properties of the aluminas are summed up in Table 1; Na introduction did not change the S.S.A. and the structure of γ-alumina. Chemical analysis was performed using ICP at the Vernaison Center of Chemical Analysis of

Table 1. Structural and Textural Properties of the Catalytic Materials Employed in This Study

	S.S.A. ($m^2 \cdot g^{-1}$)[a]	sodium content (ppm)[b]
γ −Al_2O_3	145	<50
δ −Al_2O_3	140	<50
γ −Al_2O_3 − 0,1% $NaNO_3$	138	870
γ −Al_2O_3 − 0,1% NaOH	140	900

Determined by [a]the B.E.T. method [b]elemental analysis.

DOI: 10.1021/acscatal.5b00723
ACS Catal. 2015, 5, 4423−4437

CNRS. It was verified by XPS (SPEC PHOIS BOS BOMCD5, magnesium cathode, 300 W) that sodium is not detected on γ- and δ samples but is detected for the Na-doped aluminas.

2.2. Catalytic Tests. Catalytic experiments have been carried out in a quartz fixed-bed reactor. The materials were pressed into a wafer and crushed to get a particle size between 125 and 200 μm in order to avoid diffusional limitations. A given amount of the catalyst sample (between 4 and 80 mg) was diluted in SiC (same particle size, inert toward isopropanol dehydration below 350 °C) and loaded into the reactor to form a catalytic bed of 0.1 mL (diameter: 1.00 cm, length: 0.13 cm). The axial Peclet number calculated for this reactor was close to zero (0.23), and its behavior could be approximated to that of a single Continuously Stirred Tank Reactor (CSTR) (see Supporting Information, section 2). Reaction rates were calculated accordingly.

In a typical experiment, the catalyst was activated for 3 h at 450 °C (7.5 °C·min^{-1}) under nitrogen flow (Azote U Air Liquide, 20 mL·min^{-1}) and cooled down under N_2 to the temperature of isopropanol dehydration (T = 180 to 220 °C). Isopropanol (Sigma-Aldrich, 99%) was stored in a saturator whose temperature was set to 5 °C in order to deliver a partial pressure of 1.5 kPa in the nitrogen flow (6.0 to 60.0 mL·min^{-1}). It was checked by varying the amount of catalyst loaded and the reactant flow rate that diffusion limitations were not observed in these conditions. Contact time was calculated by dividing the accessible volume (0.033 cm^3 considering a close-packing of the grains) by the volumetric flow rate. The composition of the effluent was determined by gas chromatography (Perichrom, Silocel 15% TCEPE column, T_{oven} = 60 °C, $T_{injector}$ = 200 °C, $P_{injector}$ = 80 kPa). All data reported in this paper have been recorded under steady-state conditions (Figure S3, Supporting Information). The carbon content in the inlet stream was recovered in the outlet stream up to at least 97% for any experiment, the missing content being mainly attributed to the experimental uncertainty. Only propene and diisopropylether were detected. Selectivity to diisopropylether was calculated with respect to isopropanol according to the formula

$$S_{\text{diisopropylether}} = \frac{2P_{\text{diisopropylether}}}{2P_{\text{diisopropylether}} + P_{\text{propene}}}$$

The initial dehydration rate (r_0, given in mol·m^{-2}·s^{-1}) was calculated at low contact time and low conversion (3−10%) using the highest accessible flow rate (60 mL·min^{-1}). The initial rates of production of propene and diisopropylether ($r_{0,i}$) were calculated in the same way, and the activation energies and enthalpies were measured from the dependence of $r_{0,i}$ toward temperature (in the range 160−210 °C) by use of Arrhenius and Eyring plots: ($\ln(r_{0,i}) = f(1/T)$) and ($\ln(r_{0,i}/T) = f(1/T)$), respectively—the latter allowing more precise comparison with DFT calculated values.

2.3. *Ab Initio* Calculations. *a. Settings for Electronic and Geometry Calculations.* All calculations were performed using the *ab initio* plane-wave pseudopotential method as implemented in VASP (Vienna *Ab Initio* Simulation Package).[42,43] The generalized gradient approximation exchange−correlation functional of Perdew, Burke, and Ernzerhof PBE[44] was chosen to perform the periodic DFT + D2 calculations, with dispersion forces correction from the Grimme approach.[45] In this approach, core electrons are not explicitly computed. Their interaction with the valence electrons is described by pseudopotentials from the projector augmented wave (PAW) approach,[46] while the valence electrons wave functions are projected on a set of plane waves with a cutoff energy of 400 eV. The convergence criterion for the electronic self-consistent field relaxation was fixed to 10^{-5} eV. Geometry optimizations are performed using a conjugate-gradient algorithm, with a convergence criterion on forces of 0.02 eV·Å^{-1}. In addition to the adsorbate species, the two upper atomic layers of the slab were allowed relaxing. Dipolar correction along the z axis was found to have no impact on both optimized structure and energies, and was subsequently omitted.

Harmonic frequencies calculations were performed on optimized structures with an improved cutoff energy (500 eV). The Hessian matrix was calculated by the finite difference method. The diagonalization procedure of this matrix yields the harmonic frequencies (eigenvalues) and the associated vibrational mode (eigenvectors). As for geometry optimizations, the two upper atomic layers of the slab were allowed relaxing in addition to the adsorbate.

Transition-state calculations were performed using the Nudged Elastic Bands (NEB) method,[47] with 10 images, including initial and final states. To start with, an interpolation scheme involving both Cartesian and internal coordinates is used (Opt'n-Path developed by Paul Fleurat-Lessard).[48] The calculation is then carried out in several steps: a first NEB calculation is performed, followed by a Climbing Image NEB (CI-NEB),[49] as implemented in the VTST module. The supposed transition state is then relaxed using a quasi-Newtonian algorithm[50] (E_{cutoff} = 500 eV) until convergence criteria are reached (electrons: 10^{-6} eV; nuclei: 0.01 eV·Å^{-1}). A vibrational calculation is ultimately performed to assess the reliability of the isolated transition state. It might happen that a vibrational mode with very low imaginary frequencies is calculated ($\tilde{\nu}$ < 80 cm^{-1}) in addition to the imaginary mode corresponding to the reaction coordinate, even after trying to discard it through a calculation using the DIMER method.[51] Methods for treating residual imaginary frequencies have been proposed in the literature.[52,53] We evaluated the influence of the method on the calculated enthalpies and entropies (see Supporting Information, Table S1). The choice of the method was found to have no influence on the enthalpies, while entropies may vary by up to 14 J·K^{-1}·mol^{-1}. In the present paper, the imaginary frequency was turned into a real frequency for the thermodynamic calculations.

b. Models. Calculations on gas-phase molecules (isopropanol, water, and diisopropylether) were performed on VASP by placing the molecule in a 20 Å wide box. The convergence in energy with the size of the box has been verified. γ-Alumina mainly exposes (100) and (110) surface planes. Surface models developed by Digne et al. from a nonspinel bulk structure were employed in this work.[54,55]

The (100) surface model used in the present study consists of a triperiodic cell, the size of which is 16.8 × 11.1 × 28.0 Å^3, occupied by a 6.0 Å wide alumina slab (normal to the Oz axis) surmounted by a 22 Å wide vacuum slab. The Brillouin zone integration is performed on a 1 × 2 × 1 k-points grid mesh. The (110) surface model is 16.1 × 16.8 × 28.0 Å^3 wide, occupied by a 6.0 Å thick alumina slab (normal to the Oz axis), representing four alumina layers, surmounted by a 22 Å wide vacuum slab. The Brillouin zone integration is performed on a 1 × 1 × 1 k-points grid mesh. Both surfaces are considered in a dehydrated or hydrated state, with OH-coverage increasing from 0 to 15 OH·nm^{-2}. The hydrated models were constructed by adsorbing water molecules and optimizing the structure, as performed by

DOI: 10.1021/acscatal.5b00723
ACS Catal. 2015, 5, 4423−4437

Digne et al.[54,55] For the (100) surface, no difference with their work has been found. For the (110) termination, a surface reconstruction leading to a strong stabilization for OH coverage superior or equal to 9.0 OH·nm^{-2}, as proposed by Wischert et al.,[56] was taken into account.

Figure 3 shows a top view of the elementary cell of the surfaces in their dehydrated state (Figure 3a,b) and partially hydrated state (Figure 3c,d). The (100) dehydrated surface exhibits pentacoordinated aluminum atoms, denoted $Al_{Va\text{-}c}$, as well as 3- or 4-fold coordinated oxygen atoms (noted $O_{3a\text{-}b}$ or O_4, respectively), while the (110) dehydrated surface exhibits a tricoordinated aluminum ion (Al_{III}) and tetra-coordinated aluminum ions ($Al_{IVa\text{-}b}$).

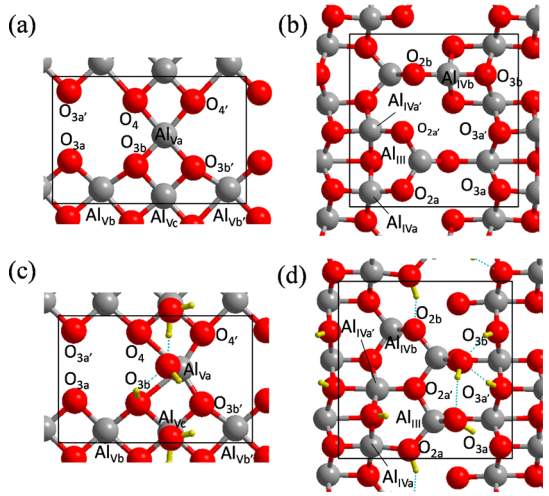

Figure 3. Elementary cells of γ-alumina surfaces: (a) dehydrated (100), (b) dehydrated (110), (c) partially hydrated (100) (8.8 OH·nm^{-2}), (d) partially hydrated (110) (8.9 OH·nm^{-2}). The frame delimits the elementary cells. We used simulation cells containing four elementary cells (2 × 2). Only the upper layer is shown on the figure. Gray: Al, Red: O, Yellow: H.

Upon hydration, water can either dissociate to form hydroxyl groups (e.g., μ_1−OH and μ_2−OH, as shown in Figure 3c,d) or adsorb in a nondissociative way at higher water coverage (Figure 3c: water molecules on the edge of the cell). Prime symbols refer to equivalent atoms in the dehydrated cells. The naming of the Al sites will be conserved when water coverage increases, even if the coordination of the atoms changes upon hydration. Finally, note that in order to limit lateral interactions effect between adsorbates, we used simulation cells doubled along the x and y axes (see caption of Figure 3).

The adsorption of a molecule A in a given mode on a given surface in a given hydration state is defined by the reaction 1:

$$A_{(g)} + \{\text{Surface}\} = \{A - \text{Surface}\} \quad (1)$$

The corresponding adsorption energy can be calculated by eq 2

$$\Delta_{ads}E(0\ \text{K}) = E(\{A - \text{Surface}\}) - E(\{A\}) - E(A_{(g)}) \quad (2)$$

where the different energies are the computed electronic and ionic energies of the different systems. The adsorption of a single isopropanol molecule corresponds to an isopropanol coverage of 0.53 and 0.37 *i*PrOH·nm^{-2} on the (100) and (110) surface models, respectively.

c. Thermodynamic Calculations. In order to assess the temperature-dependent behavior of the adsorbed water and the entropic contribution in the adsorption processes, thermodynamic calculations were carried out on adsorbed molecules. The change in any state function X (enthalpy, entropy or Gibbs free energy) associated with the adsorption reaction 1 can be calculated through the following eq 3:

$$\Delta_{ads}X(T, P) = X(\{A - \text{Surface}\})(T, P) - X(\{\text{Surface}\})(T, P) - X(A_{(g)})(T, P) \quad (3)$$

where P is the partial pressure of the gas phase species. The procedure, fully described in the Supporting Information (p 3), involves the calculation of the vibrational contributions to the internal energy and entropy of the surface systems—with or without an adsorbed molecule. These calculations also allow access to the enthalpy and entropy change during an adsorption or reaction process. In a similar way, the activation enthalpy, entropy, and free energy can be assessed by calculating the change in the given function (X) between the transition state and the initial state:

$$\Delta_r X^{\ddagger}(T) = X(\text{Transition state})(T) - X(\text{Initial state})(T) \quad (4)$$

As we only consider surface reactions, activation enthalpies, and entropies are calculated as follow:

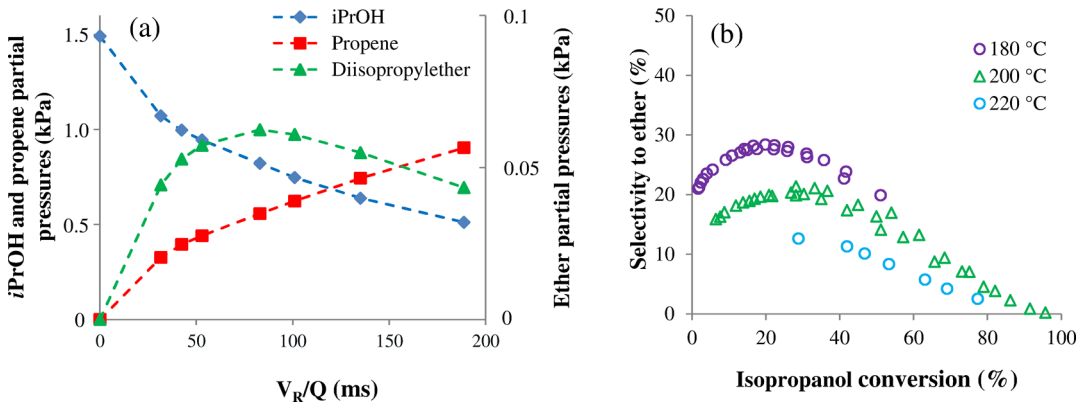

Figure 4. (a) Evolution of partial pressures with contact time (volume of the reactor V_R-to-flow rate Q ratio) for the γ−Al_2O_3 sample (reaction temperature 200 °C, initial P_{iPOH} = 1.5 kPa, m_{cata} = 30 mg, ether partial pressure is displayed on the right axis for the sake of clarity); (b) Selectivity to ether vs isopropanol conversion plot for the γ−Al_2O_3 sample at different reaction temperature (180, 200, and 220 °C).

DOI: 10.1021/acscatal.5b00723
ACS Catal. 2015, 5, 4423−4437

Table 2. Measured Activation Energies (Arrhenius Plot) and Enthalpies (Eyring Plot) for the Formation of Propene and Diisopropylether on the Different Alumina-Based Catalysts[a]

	formation of propene			formation of diisopropylether			r_0 @ 200 °C (mol·m^{-2}·s^{-1})
	E_a (kJ/mol)	$\Delta_r H^{\ddagger}$ (kJ/mol)	R^2	E_a (kJ/mol)	$\Delta_r H^{\ddagger}$ (kJ/mol)	R^2	
γ –Al_2O_3	133 ± 5	128 ± 5	0.9995	122 ± 5	118 ± 5	0.9992	$9.28 \cdot 10^{-8}$
δ –Al_2O_3	138 ± 5	134 ± 5	0.9993	126 ± 5	122 ± 5	0.9999	$4.41 \cdot 10^{-8}$
γ –Al_2O_3 – 0.1% $NaNO_3$	136 ± 5	132 ± 5	0.9998	122 ± 5	118 ± 5	0.9995	$1.72 \cdot 10^{-8}$
γ –Al_2O_3 – 0.1% NaOH	133 ± 5	129 ± 5	0.9992	120 ± 5	116 ± 5	0.9956	$1.25 \cdot 10^{-8}$

[a]Coefficient of linear regression is displayed for each material, as well as the initial rate of conversion of isopropanol r_0 at 200 °C (under steady-state). See plots in Supporting information, Figure S4.

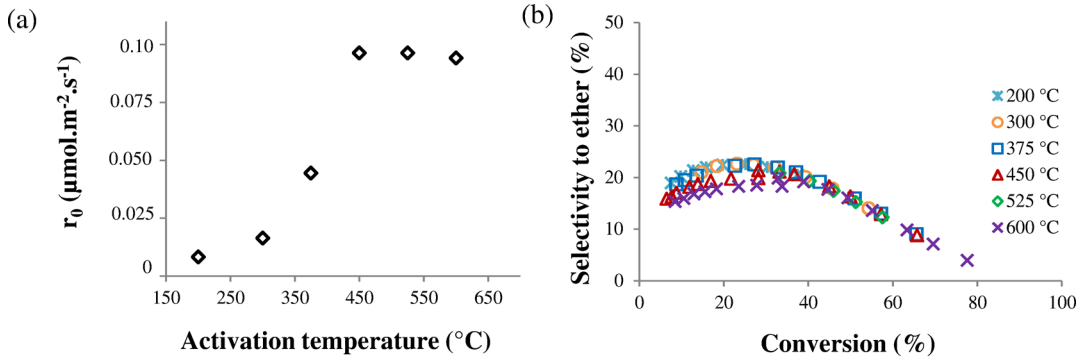

Figure 5. (a) Initial conversion rate of isopropanol r_0 on γ-Al_2O_3 activated at different temperatures. (b) Selectivity to diisopropylether vs conversion plot monitored for γ-Al_2O_3 activated at different temperatures. Reaction temperature: 200 °C; initial P_{iPOH} = 1.5 kPa. Isopropanol conversion at a given activation temperature is varied by means of contact time.

$$\Delta_r H^{\ddagger}(T) \approx \Delta_r U^{\ddagger}(T) = E^{\ddagger} - E(\mathrm{IS}) + U_{vib}{}^{\ddagger}(T) - U_{vib}(\mathrm{IS})(T)$$
$$\Delta_r S^{\ddagger}(T) = S_{vib}{}^{\ddagger}(T) - S_{vib}(\mathrm{IS})(T) \quad (5)$$

where E stands for the molar electronic and nuclear energy given by the DFT calculations, and U_{vib} and S_{vib} the molar vibrational energy and entropy, respectively, for the transition state (‡) and initial state (IS).

3. RESULTS

3.1. Experimental Results. *a. Kinetic Measurements on Pure γ-Alumina.* All results reported below have been recorded under steady-state conditions (Figure S3, Supporting Information). The evolution of partial pressures with contact time (accessible volume-to-flow rate ratio) at constant reaction temperature (200 °C) for the γ-alumina sample is shown in Figure 4a. As expected, increasing contact time causes isopropanol partial pressure to decrease. Propene partial pressure constantly increases with contact time, while diisopropylether partial pressure passes through a maximum before decreasing. As no other products are monitored, it can be assumed that diisopropylether is converted into propene and isopropanol, in line with the secondary reaction proposed by Knoezinger.[15] It can be noted that above 150 °C and in the absence of kinetic limitations, thermodynamic calculations indicate that the system should evolve to 100% isopropanol conversion and 100% selectivity to propene (thermodynamic calculations are presented as Supporting Information, Figure S2).

Figure 4b displays the selectivity to ether as a function of the isopropanol conversion, recorded for different reaction temperatures (180, 200, and 220 °C). Low conversions could not be accessed at 200 and 220 °C due to the very low mass of catalyst and high flow rate that would be required. For the experiment at 200 °C (respectively 180 °C), this selectivity increases from around 10% (respectively 20%) up to a maximum around 20% (respectively 30%) for an isopropanol conversion of 30% (respectively 25%), and then decreases to the benefit of propene. Extrapolation at zero conversion at 180 °C leads to nonzero selectivities both for propene and ether (81 and 19%, respectively), which shows that both products are formed from isopropanol through direct pathways at short contact times. Increasing the temperature decreases the selectivity to ether, which is consistent with previous observations.[15,34]

On the basis on these experiments, the apparent activation energies for the two direct dehydration routes were determined below 8% of conversion, assuming that the secondary reaction has little effect at low isopropanol conversion (Table 2). The formation of diisopropylether is slightly less activated (122 kJ·mol^{-1}) than the formation of propene (130 kJ·mol^{-1}), although it is the minor product of the reaction. This is in line with the observed temperature dependence of the selectivity.

These results confirm that at least three steps are necessary to fully describe the dehydration of isopropanol: the two direct routes for the formation of diisopropylether and propene, and the secondary reaction of diisopropylether conversion evidenced at longer contact time. At a given temperature, the position and value of maximum selectivity to ether as a function of isopropanol conversion should thus depend on the respective rates of these three steps. These rates are themselves functions of intrinsic reaction rates, characteristic of the active sites, and of the surface concentration of active sites. We adopted three strategies to vary the concentrations of these active sites:

- Changing the surface hydration state by changing the temperature of alumina activation;
- Changing the proportion of surface planes by switching to another transition alumina;

DOI: 10.1021/acscatal.5b00723
ACS Catal. 2015, 5, 4423–4437

– Modifying the surface properties of γ-alumina by a chemical poisoning by sodium.

The kinetic study was carried out at the same reaction temperature in all cases (200 °C), so that the intrinsic rate constants characteristic of each site should not be modified between the different experiments.

b. Influence of the Activation Temperature. Changing the activation temperature is expected to modify the surface hydroxylation state, an increase in temperature leading to surfaces that expose a smaller number of OH groups and a larger number of Lewis acidic sites. The activation temperature was varied between 200 and 600 °C. Figure 5a shows that the initial isopropanol dehydration rate at 200 °C (measured under steady-state conditions at low contact time and low conversion) increases with the activation temperature, being low when surfaces are originally highly hydroxylated, and reaching its maximum value for an activation temperature of at least 450 °C. This observation raises the question of preadsorbed water acting as an inhibitor for isopropanol conversion. Conversions are stable with time on stream, which indicates that water produced by the reaction does not accumulate on active sites. OH groups remaining after an activation at low temperature seem to have a different effect, as isopropanol is not able to displace them—otherwise activity should be ultimately leveled whatever the initial activation temperature. Cooperative effects, such as strong hydrogen bonding between neighboring OH groups, may be invoked to account for their stabilization on the surface.

Figure 5b shows, however, that the selectivities are similar whatever the activation temperature. Changes in OH coverage thus affect in a similar way the three routes listed above, which we may suppose involve dehydrated sites.

c. Kinetic Measurements on δ-Alumina. We then examined the influence of the exposed crystallographic terminations of the alumina. For this purpose, we chose a commercial δ-alumina of similar surface specific area. δ-Alumina is known to result from the sintering of γ-alumina particles through the lateral (100) facets of the crystallites.[57] δ-Alumina thus exhibits a (100)/(110) surface ratio smaller than that of γ-alumina. From now on, the alumina activation temperature will be 450 °C in all cases, as was initially chosen for γ-alumina.

Table 2 shows the results of the measurements of the catalytic activity on δ-alumina. Compared with γ-alumina, the initial isopropanol conversion rate is smaller by a factor of 2 on δ-alumina, in line with previous observations by Narayanan et al.[58] However, the measured activation energies for the formation of both propene and diisopropylether are very similar to those of γ-alumina, in the range of the experimental uncertainty. Moreover, selectivities are not modified (Figure 6), and the same partial pressure evolution is monitored (Supporting Information, Figure S5). We verified that this behavior is also observed at 180 °C (see Supporting Information, Figure S6). This provides evidence of a similarity of active sites between the two aluminas for the three reaction routes. As the overall activity strongly decreases when the (100)/(110) ratio decreases, it may be inferred that the active sites are rather located on the (100) planes.

d. Kinetic Measurements on Na-Poisoned γ-Aluminas. Finally, we examined the effect of a chemical poisoning of the γ-alumina surface. Sodium ions are well-known to be poisons which severely inhibit alcohols dehydration.[59,60] Two precursors were used to introduce sodium (NaOH and $NaNO_3$),

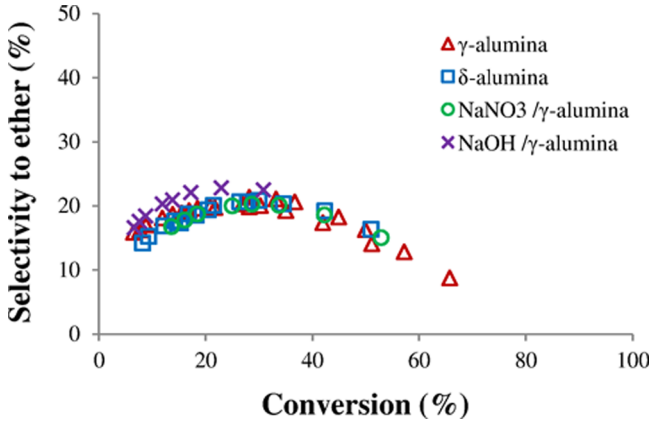

Figure 6. Selectivity to diisopropylether vs conversion plot monitored with alumina-based catalysts: γ-alumina, δ-alumina, and sodium-poisoned γ-alumina. Reaction temperature: 200 °C ; initial P_{iPOH} = 1.5 kPa.

with only little difference between the overall behavior of the two resulting doped aluminas, indicating that the sodium content is the determining parameter. No other products, except for propene and diisopropylether, were detected. The catalytic activity and the activation energies of the primary reactions were assessed (Table 2 and Figure 6, as well as Figure S7 of the Supporting Information). Although the initial reaction rate strongly decreases (by a factor of 9), selectivity as a function of conversion is barely modified compared with pure alumina. Sodium thus affects the active sites to the same extent for all the routes involved in isopropanol dehydration.

Three conclusions can be drawn from this series of experiments. First, at a given temperature, the intrinsic rates of each route involved in isopropanol dehydration are similar for all the aluminas tested, whatever the alumina modification, with the same activation energies for propene and diisopropylether formation. Second, it is rather the number of active sites involved in these routes that seem to change; it decreases with Na-poisoning and increases with surface dehydration and with the exposure of (100) facets. Third, it is important to note that poisoning by adsorbed OH groups or Na^+ ions does not affect one route more than the others, because the same proportion of propene and diisopropylether is always obtained at a given conversion. We thus suggest that the three reaction routes (direct formation of alkene and ether, decomposition of ether) actually occur on a set of adjacent active sites, possibly involving Lewis acidic sites on (100) terminations. In the next part, we will verify the plausibility of this hypothesis, by investigating the adsorptive and catalytic properties of various surface sites present on γ–alumina (100) and (110) surfaces through a molecular modeling approach.

3.2. Computational Results. *a. Initial Surface Hydration State.* In order to determine the initial hydration state of the (100) and (110) planes terminations of γ-alumina after activation, thermodynamic considerations are presented in a first stage. Digne et al.[54,55] have developed molecular models for the surfaces of γ-alumina, and calculated the successive adsorption energies of water molecules on these models. Using statistical thermodynamics considerations, Joubert et al. obtained the expressions of the fraction of surface cells occupied by a given amount of water molecules.[61,62] We performed a similar analysis (fully developed in the Supporting Information, pp 10–11) using calculated adsorption enthalpies

DOI: 10.1021/acscatal.5b00723
ACS Catal. 2015, 5, 4423–4437

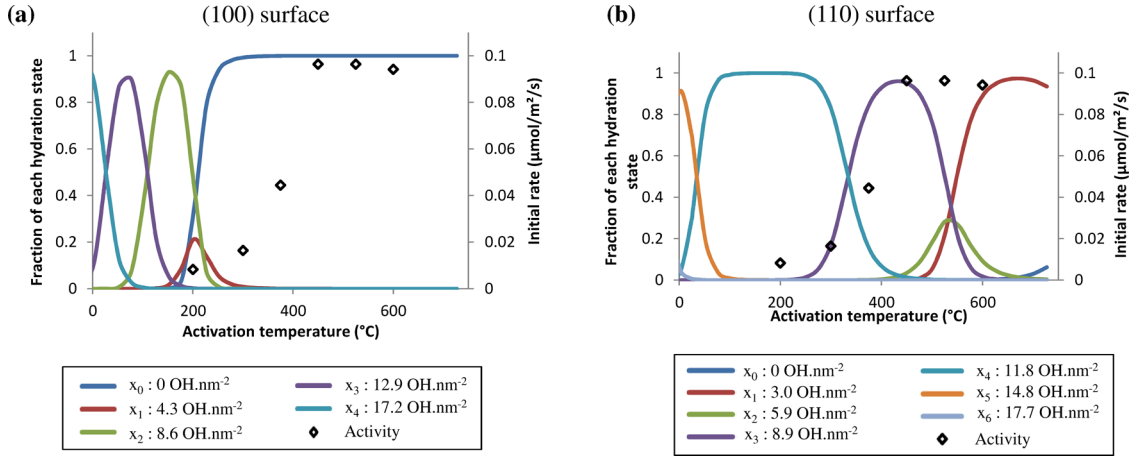

Figure 7. Evolution of the thermodynamic hydration state with temperature (a) (100) surface, (b) (110) surface. $P_{H_2O} = 10^{-3}$ bar. x_i is the fraction of elementary cells that contain i water molecules.

and entropies of adsorbed water molecules on the γ-alumina surface elementary cells. Given the nature of the surface aluminum atoms of the (100) and (110) surfaces, the elementary cell of the (100) surface can accommodate up to four water molecules while (110) can accommodate up to 6 water molecules. We will note x_i the proportion of elementary cells that contain i water molecules. The corresponding local OH surface density will be given in Figure 7.

We considered the water partial pressure during the activation under nitrogen flow to be of 10^{-3} bar. This water partial pressure is also representative of the reaction conditions, provided that the conversion of isopropanol remains lower than 5%. The speciation diagrams for the surface hydration as a function of activation temperature are shown in Figure 7.

The initial reaction rate of isopropanol dehydration as a function of the activation temperature is superimposed to these plots. It appears that the maximum activity corresponds to a dehydrated (100) surface (x_0), or to a partially hydrated (110) surface containing around 8.9 OH·nm^{-2} (x_3). The corresponding models have been used in the following sections for the reaction pathway calculations.

*b. Isopropanol Reactivity on the (100) Dehydrated Surface. *. Propene Formation.* The dehydrated (100) surface exposes three nonequivalent aluminum atoms (see Figure 3a), on which isopropanol can be adsorbed by forming an Al−O bond. The enthalpies and entropies of adsorption on these sites are given in Table 3. Isopropanol preferentially adsorbs as a deprotonated alcoholate on the Al_{Va} site (−121 kJ·mol^{-1}), a stabilizing (10 kJ·mol^{-1}) and very slightly activated process (3 kJ·mol^{-1}), as shown in Figure 8. On the other sites (Al_{Vb} and Al_{Vc}), the adsorption is less favorable (−88 and −89 kJ·mol^{-1}, respectively) and the dissociation of the O−H bond is no longer stabilizing. We verified that the competitive adsorption between water and isopropanol is in favor of isopropanol by around 15−20 kJ·mol^{-1} on all aluminum sites of the (100) surface. Isopropanol adsorption is not prevented by the presence of water in the gas phase at low conversion, in line with the absence of deactivation with time-on-stream.

Four different mechanisms can be proposed for the formation of propene (Figure 2):[63]

- E1: mechanism in two steps, in which the C−O bond breaks in the first step, forming a carbocation intermediate, before the β C−H bond breaks to yield propene.
- $E1_{cb}$: mechanism in two steps, in which the β C−H bond breaks in the first step, forming a carbanion intermediate, before the C−O bond breaks to yield propene.
- E2: concerted mechanism in which the C−O and β C−H bonds break simultaneously to yield propene without any intermediate species.
- An intramolecular concerted elimination—referred to as $E2_{intra}$ in the present paper—was also investigated. In this mechanism, the β hydrogen atom is transferred to the oxygen atom of the alkoxide itself while the C_α−O bond breaks. This mechanism was proposed in a previous study by Kwak et al.,[36] and referred to as "E1", although it does not correspond to the usual definition of a two-step E1 mechanism.[63]

Table 3. Isopropanol Adsorption and Activation Parameters for the Formation of Propene Following the E1, E2, and $E1_{cb}$ Mechanisms on the (100) Surface of γ-Alumina[a]

site	adsorption		reactivity			
	$\Delta_{ads}H°$	$\Delta_{ads}S°$	mechanism	$\Delta_rH^‡$	$\Delta_rS^‡$	$\Delta_rG^‡$
Al_{Va}	−121	−186	E1	201	+15	197
			E2	125	−8	129
			$E1_{cb}$	147	−43	167
Al_{Vb}	−88	−200	E2	146	+14	139
			$E1_{cb}$	141	−30	155
Al_{Vc}	−89	−194	E2	125	−4	127
			$E1_{cb}$	125	−36	142

[a]For the two-step mechanisms (E1 and $E1_{cb}$), the reported data concern only the first step. Enthalpies are given in kJ·mol^{-1}, entropies in J·K^{-1}·mol^{-1}, and are calculated at 200 °C.

It should be first recalled that in the case of isopropanol adsorption on Al_{Va}, both the breaking of the O−H bond of the alcohol leading to a stable, dissociated alkoxide, and the reverse process are only slightly activated. As the O and H atoms remain very close to each other, adsorbed protonated and deprotonated alcohols can be considered at equilibrium, yet strongly in favor of the dissociated state; thermodynamic calculations indicate that roughly 94% of the total adsorbed fraction should be in the dissociated state. The latter was considered as the initial state for propene formation on this site,

DOI: 10.1021/acscatal.5b00723
ACS Catal. 2015, 5, 4423−4437

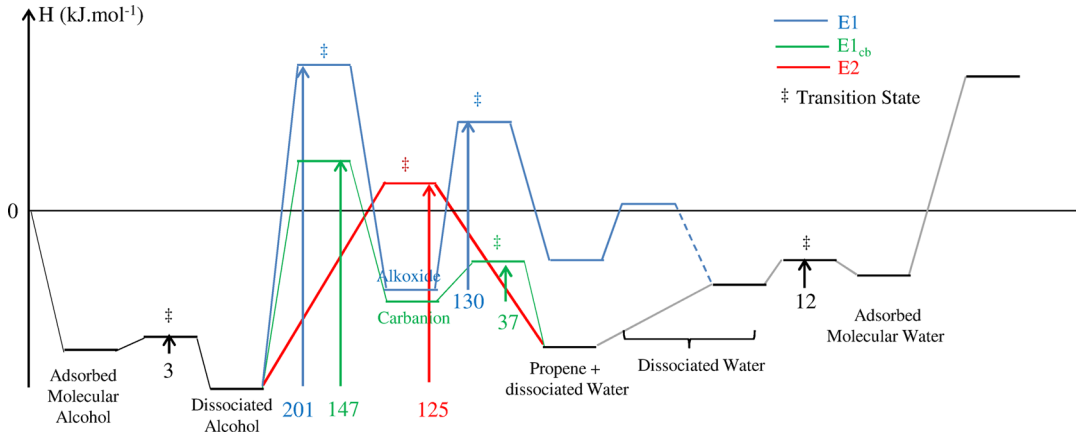

Figure 8. Enthalpic diagram for the formation of propene on the Al_{Va} site of the (100) surface (the corresponding diagrams for entropy and free energy are available in the Supporting Information, Figures S8−S10 and S13). Note: for the E1 mechanism, the surface is left with a dissociated water molecule in a highly unfavorable state after desorption of the propene molecule. We consider that the system spontaneously evolves to the much more favorable dissociated molecule similar to the one obtained by the E2 and $E1_{cb}$ mechanisms (dotted step).

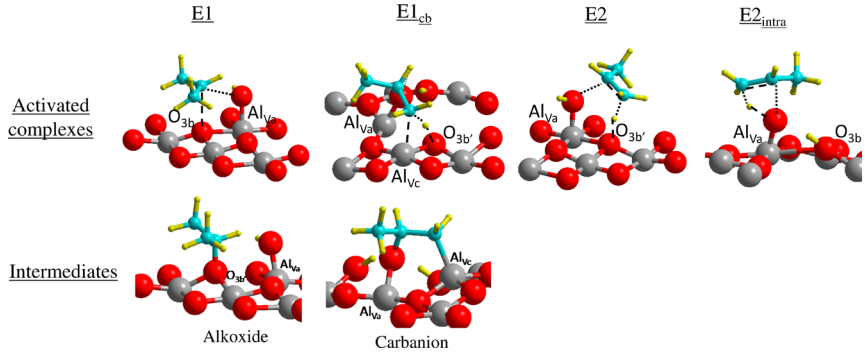

Figure 9. Calculated transition states (first step only) and intermediates for the E1, $E1_{cb}$, E2, and $E2_{intra}$ mechanisms of the formation of propene, on the Al_{Va} site of the (100) terminations. --- represents a forming bond, while ···· stands for a breaking bond. Same color code as Figure 3, with blue representing carbon. Additional activated complexes structures can be found in the Supporting Information, Figure S15.

but it will appear below that the proton may easily reassociate with the O atom during the transition state formation. However, a transient protonated alcohol intermediate was never isolated during the NEB research. For these reasons, and for a better comparison between DFT and experimental results, we considered that the temperature dependency of the rate constant would depend on the enthalpic difference between the transition state and the most stable initial state, and not between the transition state and the initial state exhibiting the closest structure. In the case of the Al_{Va} site only, we thus calculated the activation parameters from the difference between the transition state and the dissociated adsorbed alcohol. We refer here to the energetic span concept[64,65] and demonstrate this point in Supporting Information, section 7.

Figure 8 presents the calculated evolution of enthalpy for the main steps of the formation of propene on the Al_{Va} site of the (100) surface. Recombination of the water fragments as well as desorption of propene and water are also shown. It was checked from the free energy diagrams (see Figures S8−S10 of the Supporting Information) that none of these steps is kinetically determining. In particular, the recombination of water is very poorly activated (12 kJ·mol^{-1}), in a similar way as the dissociation of isopropanol. The corresponding evolution of entropy and free energy of these processes is given in Supporting Information (Figure S8−S10 and S13).

For the two-steps mechanisms (namely, E1 and $E1_{cb}$), the formation of the intermediate (alkoxide or carbanion, respectively) is expected to be the kinetically determining step, and the value given for the activation barrier correspond to the first step. This is visible on the enthalpic diagram concerning the Al_{Va} site (Figure 8).

The carbocation intermediate resulting from the E1 mechanism cannot be stabilized by the surface; it spontaneously evolves into a new surface alkoxide by bonding to a surface oxygen atom, with a very high activation enthalpy (201 kJ·mol^{-1} starting from isopropanol adsorbed on the Al_{Va} site). The very unstable transition state found (Figure 9) resembles a carbenium ion. The poor stability of carbenium ions on alumina was formerly mentioned for ethanol.[38] Carbenium chemistry requires stabilization of strongly charged species, which is possible in microporous aluminosilicates thanks to the high electrostatic field within the microporosity,[66,67] but becomes irrelevant for planar alumino-silicates.[67] As a consequence, the E1 mechanism is considered to be very unlikely compared to the others and will not be considered on the other Al_V sites. Likewise, elimination through a $E2_{intra}$ mechanism is discarded on the basis of very high activation barriers (above 250 kJ·mol^{-1}). Note that the formation of propene and water by this mechanism yields a water molecule split on two separate Al and O atoms, which is very unfavorable. We consider that this state evolves spontaneously to the much more favorable state in

DOI: 10.1021/acscatal.5b00723
ACS Catal. 2015, 5, 4423−4437

which the water fragments are adsorbed in strong interaction with each other on adjacent Al and O atoms (see dotted step in Figure 8).

Activation enthalpies found for the formation of propene following the $E1_{cb}$ and E2 mechanisms on the different sites of the (100) surface are given in Table 3, together with the corresponding thermodynamic parameters calculated at 200 °C. The discrimination between the E2 and $E1_{cb}$ mechanisms is quite difficult on the sole basis of the activation enthalpies, as calculated values belong to the same range (125 to 147 kJ·mol^{-1}). However, the activation entropy for a E2 mechanism is close to 0 J·K^{-1}·mol^{-1} (from −8 to +14 J·K^{-1}·mol^{-1}) while it is significantly more negative for a $E1_{cb}$ mechanism (between −43 and −30 J·K^{-1}·mol^{-1}), leading to a more entropically activated process. Actually, the $E1_{cb}$ mechanism involves a pseudopenta-coordinated carbon atom during the breaking of the C−H bond (formation of a C−Al bond), whereas during E2 elimination, the tetrahedral carbon atom evolves into a less constrained trigonal atom. Hence, while $E1_{cb}$ is enthalpically competitive with E2 elimination, it is entropically disfavored. As a consequence, Gibbs free energies of activation are systematically lower for E2 mechanisms. Finally, despite its quite favorable activation entropy, the E1 mechanism remains the most unlikely route of all, considering its high free energy of activation.

It can be pointed out that the less activated routes (E2 or $E1_{cb}$) involve a particular surface oxygen atom, namely, O_{3b} or $O_{3b'}$, which seems particularly efficient at withdrawing the β-hydrogen atom of isopropanol. These oxygen atoms are originally tricoordinated, but upon hydrogen abstraction, the Al_{Va}-$O_{3b\ or\ b'}$ bond breaks and a μ_2−OH group is formed. On the contrary, the reaction does not seem to be very sensitive to the nature of the Al_V acidic Lewis site—even if Al_{Vb} is slightly less reactive than Al_{Va} and Al_{Vc} (Table 3). We note, however, that Al_{Va} appears both as the strongest adsorption site and exhibits one of the lowest activation enthalpies for reaction.

Finally, we chose to check the influence of surface hydration, by assuming that the (100) surface would still retain some OH groups after thermal activation. We first investigated the possibility of a mechanism involving an acidic Brønsted site. It was not possible to stabilize a protonated alcohol intermediate as the acidic proton was always transferred back to the surface during the geometry optimization. A E2-like mechanism similar to the early proposal by Knoezinger,[21] in which the acidic proton is transferred to the alcohol while the β-hydrogen atom is withdrawn by the surface, was instead modeled (see Supporting Information, Figure S18), but the activation enthalpies were very high (above 200 kJ·mol^{-1}), making this mechanism very unlikely.

As Brønsted acidic sites on γ-alumina are generated by the dissociation of a water molecule on a Lewis acid−base pair, surface basic OH-groups also appear on the surface and may act as base centers required for the elimination of the β-hydrogen atom of the alcohol. Such possibilities have been investigated (Supporting Information, Figure S18). The formation of propene takes place through a Lewis-acid catalyzed E2 mechanism, with activation enthalpies close to the barriers found on the dehydrated surface (126 kJ·mol^{-1}). Hydroxyl groups thus might be involved in the dehydration process, but their presence is not required in order to catalyze the reaction. It can be noted that the difference between dehydration barriers using oxygen atoms or μ_1−OH groups as basic centers was formerly found to be larger (roughly 20 kJ·mol^{-1}).[40] However, in the latter case, a small cluster was used to describe the surface, and the alcohol molecule and the basic OH group were coordinated to the same aluminum atom, introducing additional inductive effects.

*. *Diisopropylether Formation.* According to the organic chemistry literature,[63] two different mechanisms can be proposed for the formation of diisopropylether from isopropanol (see Figure 2):

- S_N1: mechanism in two steps, in which the C−O bond breaks in the first step, forming a carbocation intermediate, before the second alcohol molecule reacts with the carbocation fragment to yield the ether.
- S_N2: mechanism in one step, in which the addition of the nucleophilic alcohol molecule and the elimination of the leaving OH group of the electrophilic alcohol molecule take place simultaneously.

As already shown for the E1 mechanism, the formation of the carbocation intermediate is highly activated, making the S_N1 mechanism unlikely. Only the S_N2 mechanism is considered below.

An isopropanol molecule first adsorbs on one of the aluminum atoms of the surface with the adsorption parameters given in Table 3. The second molecule can either adsorb on another aluminum atom, or on an oxygen atom through weak interactions. The different data gathered in each case for the adsorption of the second molecule and the activation parameters of the subsequent reaction are reported in Table 4.

Table 4. Activation Parameters for the S_N2 Reaction Pathways Calculated on the (100) Surface[a]

1st adsorbed *i*POH	2nd adsorbed *i*POH			reactivity			
site	site	$\Delta_{ads}H°$	$\Delta_{ads}S°$	OCO angle	$\Delta_rH^‡$	$\Delta_rS^‡$	$\Delta_rG^‡$
Al_{Va}	Al_{Vc}	−79	−171	109	214	+14	207
	Al_{Vb}	−90	−185	143	179	−39	197
	$O_{3a'}$	−62	−145	152	112	−36	129
Al_{Vb}	Al_{Vb}	−55	−155	157	206	−36	223
	Al_{Vc}	−93	−159	128	210	−3	211
	$O_{3a'}$	−62	−143	154	131	−40	150

[a]Energies and enthalpies are given in kJ·mol^{-1}, entropies in J·K^{-1}·mol^{-1}, and are calculated at 200 °C. Angles relate to the activated complex and are given in degrees.

Whatever the initial configuration, the optimized activated complexes represented in Figure 10 are typical of a S_N2 mechanism. In all cases, the electrophilic carbon atom is in a pseudo trigonal bipyramid geometry with CH_3−C−H angles close to 120°.

When the two isopropanol molecules are adsorbed on adjacent aluminum atoms (Al_{Va}/Al_{Vc} or Al_{Vb}/Al_{Vc}), the adsorption on the second site (electrophilic molecule) is slightly disfavored because of steric interactions, leading to a distorted activated complex (OCO angle =109 to 128°; see Figure 10a). The activation enthalpy is very high (214 and 210 kJ·mol^{-1}). As the electrophilic carbon is weakly constrained in this configuration, the activation entropy is close to zero (+14 and −3 J·K^{-1}·mol^{-1}), and the entropic correction is minor. The resulting free energy of activation is thus very high (207 and 211 kJ·mol^{-1}, respectively).

In the Al_{Va}/Al_{Vb} case (Figure 10-(b)), the two alcohol molecules are adsorbed on more distant aluminum atoms. Like

DOI: 10.1021/acscatal.5b00723
ACS Catal. 2015, 5, 4423−4437

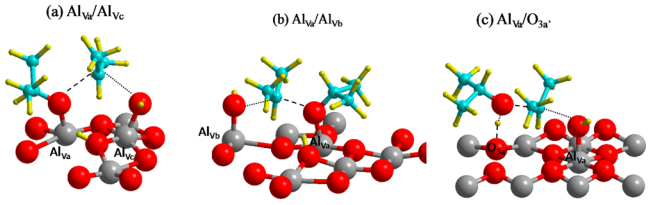

Figure 10. Activated complexes for the formation of diisopropylether on the (100) facets: (a) nucleophilic alcohol on Al_{Va} and electrophilic alcohol on Al_{Vc}, (b) nucleophilic alcohol on Al_{Va} and electrophilic alcohol on Al_{Vb}, (c) nucleophilic alcohol on $O_{3a'}$ and electrophilic alcohol on Al_{Va} --- represents a forming bond, while ●●●● stands for a breaking bond. Same color code as Figure 9. Additional activated complexes structures can be found in the Supporting Information, Figure S16.

in the first mechanism, the isopropanol molecule adsorbed on the Al_{Va} site is dissociated and acts as the nucleophilic species, while the second, nondissociated alcohol molecule acts as the electrophilic one. This mechanism has been proposed to be the most favorable by Christiansen et al. in the case of ethanol.[38] In the case of isopropanol, however, the geometry adopted by the activated complex in order to minimize steric repulsions exhibits a OCO angle of 143°, approaching a bipyramidal symmetry with a pseudopentacoordinated carbon atom. A quite high activation enthalpy (179 $kJ{\cdot}mol^{-1}$) associated with a negative activation entropy (-39 $J{\cdot}K^{-1}{\cdot}mol^{-1}$) is calculated, which yields a free energy of activation of 197 $kJ{\cdot}mol^{-1}$, only slightly lower than in the first hypothesis. Figure 11 gives a representation of the enthalpic evolution along this reaction pathway (green path). The full description, including evolution of the entropy and Gibbs free energy, is given in Supporting Information (Figures S11–S12 and S14).

The most favorable mechanism found on the (100) surface is similar to a model proposed by Jain and Pillai.[31] It involves an isopropanol molecule strongly adsorbed on an Al site, which now acts as the electrophilic species, and a weakly bound isopropanol molecule, acting as the nucleophilic species (the corresponding adsorption site is noted "$O_{3a'}$"). This basic oxygen atom assists the withdrawal of the proton from the OH group. Although the adsorption of this second molecule is not as strong as in the former mechanisms, the activation enthalpies ($Al_{Va}/O_{3a'}$ and $Al_{Vb}/O_{3a'}$) are the lowest found on this surface (112 and 131 $kJ{\cdot}mol^{-1}$, see Figure 11, red path), while the activated complexes are allowed to relax with quite wide OCO angles (152 and 157°, Figure 10c). The activation entropy for these cases is also negative (-36 and -40 $J{\cdot}K^{-1}{\cdot}mol^{-1}$), but the free energies of activation remain the lowest in the series (129 and 150 $kJ{\cdot}mol^{-1}$).

It should be added that it would be more delicate to apply the energetic span model in the case of the bimolecular diisopropylether formation (by which we should start from the most stable adsorption configuration, Al_{Va}/Al_{Vb}, Figure 10b) than in the case of the dehydration to propene, which requires a single adsorption site. As a matter of fact, there is no evidence of a simple interconversion between isopropanol adsorbed on Al_{Vb} and O_{3b}, and a simultaneous adsorption of an additional water or isopropanol molecule on unoccupied Al_{Vb} (as a strong adsorption site) that would block this site cannot be excluded. We thus preferred to consider the two initial adsorption modes and the two reaction pathways as clearly distinct, and we did not apply the energetic span model in this case.

In conclusion, comparison with the former section shows that the Al_{Va} site not only favors isopropanol adsorption but also provides the most favorable pathways for both dehydration reactions. The best activation enthalpy found on this active site is lower for the formation of diisopropylether than for the formation of propene (112 $kJ{\cdot}mol^{-1}$ vs 125 $kJ{\cdot}mol^{-1}$) but the activation entropies are in favor of the formation of the latter (-36 $J{\cdot}K^{-1}{\cdot}mol^{-1}$ vs -8 $J{\cdot}K^{-1}{\cdot}mol^{-1}$). As a result, the Gibbs free energy of activation at 200 °C for the formation of diisopropylether is in the same range as for the formation of propene (129 $kJ{\cdot}mol^{-1}$ in both cases). We note that both mechanisms involve a common adsorbed alcohol molecule. The path for the formation of diisopropylether also requires the adsorption of a second alcohol molecule which is weakly adsorbed ($\Delta_{ads}H° = -62$ $kJ{\cdot}mol^{-1}$ vs -121 $kJ{\cdot}mol^{-1}$ for the first adsorbed molecule). This may imply a smaller coverage for this second alcohol molecule and thus explain a lower rate for the formation of diisopropylether. We propose from these

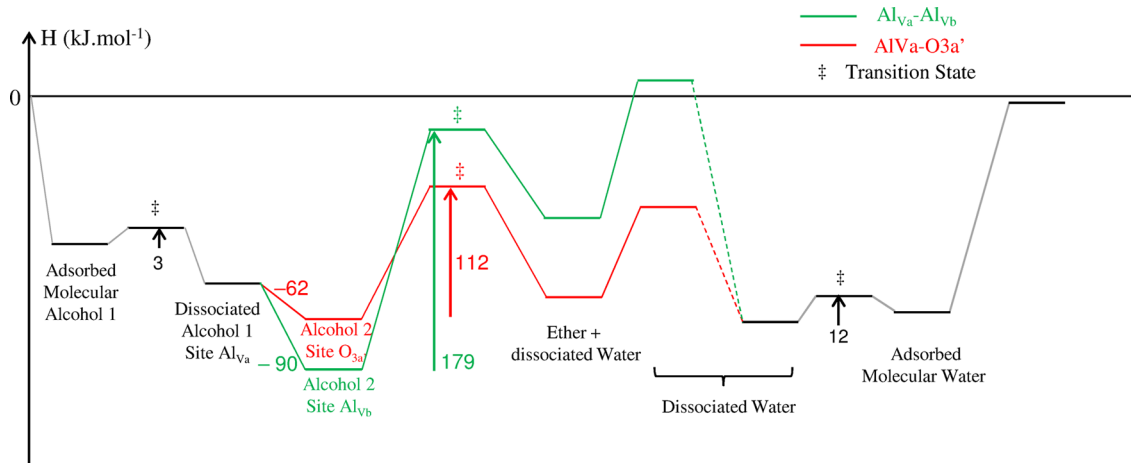

Figure 11. Enthalpic diagram of two relevant pathways for the ether formation on the (100) facets: two strongly adsorbed alcohol molecules (Al_{Va}/Al_{Vb}, green path); one strongly and one weakly adsorbed alcohol molecule ($Al_{Va}/O_{3a'}$, red path, more favorable). Entropy and free energy diagrams are available in Supporting Information (Figure S11–S12 and S14). As in Figure 8, the dotted line corresponds to a proton transfer from a dissociated water molecule to a much more stable form. Note that the free energy diagram reveals that the formation of the transition state to the ether is indeed the rate-determining step (Figure S14).

DOI: 10.1021/acscatal.5b00723
ACS Catal. 2015, 5, 4423–4437

Table 5. Calculated Adsorption and Reactivity Parameters for the Formation of Propene and Diisopropylether on the (110) Termination with a OH coverage of 8.9 OH·nm^{-2}[a]

site	adsorption		reactivity			
	$\Delta_{ads}H°$	$\Delta_{ads}S°$	mechanism	$\Delta_rH^‡$	$\Delta_rS^‡$	$\Delta_rG^‡$
Al_{IVa}	−122	−153	E2/propene	164	−16	172
$Al_{IVa'}$	−136	−201	E2/propene	158	+14	151
$Al_{IVa'}$/ Al_{IVa}	−136/−80	−201/−186	S_N2/ether	251	+6	248
Al_{IVa}/O_{3a}	−122/−54	−153/−213	S_N2/ether	130	−14	142

[a]Enthalpies are given in kJ·mol^{-1}, entropies in J·K^{-1}·mol^{-1}.

results that the lower selectivity for diisopropylether originates both from the weak adsorption of the second alcohol molecule and from the entropic effect on the intrinsic constant.

*. *Diisopropylether Conversion into Isopropanol and Propene.* As evidenced in section 3.1, and in line with previous studies,[15] diisopropylether is converted in isopropanol and propene at longer contact times, possibly on the same type of active sites as isopropanol dehydration. Because the Al_{Va} Lewis acidic site appears as the most favorable one for the formation of both propene and diisopropylether, we verified if reaction pathways for the conversion of diisopropylether, through a E2 mechanism similar to the one followed by the alcohol in its conversion to propene, could take place on this site. Adsorption parameters for the most stable structure have been found to be $\Delta_{ads}H°$ = −127 kJ·mol^{-1} and $\Delta_{ads}S°$ = −206 J·K^{-1}·mol^{-1} (see Figure S18, Supporting Information). Activation parameters are found in the same range as for the two direct reactions ($\Delta_rH^‡$ = 118 kJ·mol^{-1}, $\Delta_rS^‡$ = −16 J·K^{-1}·mol^{-1}), supporting what we consider as a plausible route for this secondary reaction.

The reverse reaction consists of the formation of diisopropylether from isopropanol and propene. The corresponding activation parameters ($\Delta_rH^‡$ = 80 kJ·mol^{-1}, $\Delta_rS^‡$ = −49 J·K^{-1}·mol^{-1}) do not allow us to exclude this possibility. However, this route supposes a preadsorbed propene molecule, which is very weakly adsorbed on the γ-alumina surface ($\Delta_{ads}H°$ = −30 kJ·mol^{-1}, $\Delta_{ads}S°$ = −140 J·K^{-1}·mol^{-1}) and thus unlikely to be found at 200 °C.

c. Isopropanol Reactivity on the (110) Surface. In the initial conditions of reaction, the relevant OH coverage for the (110) surface is assessed as 8.9 OH·nm^{-2} (section 3.2a). The surface reconstruction proposed by Wischert et al.[56] leaves this surface with only two pentacoordinated hydrated aluminum atoms exposed (Al_{IVa} and $Al_{IVa'}$). The adsorption of a single isopropanol molecule on these sites is still possible and is slightly stronger than on the (100) surface ($\Delta_{ads}H°$ = −122 and −136 kJ·mol^{-1} versus −121 kJ·mol^{-1} at best). As no carbanion intermediate could be optimized on this surface, the only examined mechanism for the formation of propene was E2. The calculated activation parameters are reported in Table 5, and the structures of the corresponding activated complexes are shown in Figure 12. On both sites, the activation enthalpies found for the formation of propene are significantly higher than for the most likely pathways found on the dehydrated (100) termination (164 and 158 kJ·mol^{-1}, vs 125 kJ·mol^{-1} at best on the Al_{Va} and Al_{Vc} of the (100) termination).

On the two nonequivalent Lewis acidic sites accessible to isopropanol (Al_{IVa} and $Al_{IVa'}$), the only available basic groups are surface oxygen atoms. In order to investigate the possible abstraction of the β-hydrogen atom by a μ_1−OH group, we had to consider the less stable surface from Digne et al.[54] without taking the improvements proposed by Wischert et al. into account.[56] Activation enthalpies were found to be 160 kJ·mol^{-1}

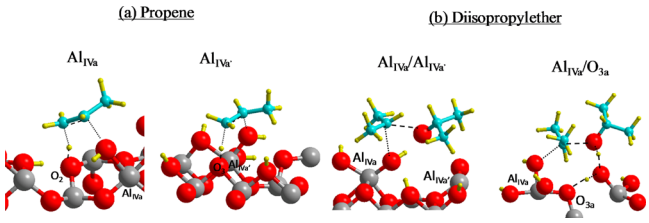

Figure 12. Activated complexes for the formation of (a) propene and (b) diisopropylether on the (110) surface. --- represents a forming bond, while ●●●● stands for a breaking bond.

(see Supporting Information, Figure S18), which is very close to the barrier found when surface oxygen atoms are the basic centers. As concluded above on the (100) surface, OH groups may be involved in the reaction, but their presence is not necessary to explain the mechanism and does not change the dehydration process significantly. In any case, activation barriers are larger on the (110) surface than on the (100) facets.

The mechanisms for the formation of diisopropylether have also been studied. Two paths were considered:

- The first one involves two isopropanol molecules adsorbed on Al_{IVa} and $Al_{IVa'}$. In this case, the two molecules are so close to each other that the adsorption of the second one is weakened (−73 kJ·mol^{-1}, against −122 on the same site without the first molecule adsorbed), preventing the "classical" S_N2 mechanism (antiperiplanar transition state). A syn-periplanar substitution (addition of the nucleophilic moiety and departure of the leaving group *on the same side* of the electrophilic carbon atom) is possible but it is a highly activated process ($\Delta_rH^‡$ = 251 kJ·mol^{-1}).
- The second one is similar to the most interesting one found on the (100) termination. The electrophilic alcohol molecule is adsorbed on the Al_{IVa} site, while the nucleophilic molecule is weakly adsorbed by hydrogen bonding to two neighboring μ_1−OH groups ($\Delta_{ads}H°$ = −54 kJ·mol^{-1}, $\Delta_{ads}S°$ = −213 J·K^{-1}·mol^{-1}). Diisopropylether is formed with an activation enthalpy of 130 kJ·mol^{-1}, the hydrogen atom from the nucleophilic alcohol being transferred to the O_{3a} oxygen atom of the surface via one of the μ_1−OH groups.

The formation of propene induces activation entropies close to 0 (here between −16 and +14 J·K^{-1}·mol^{-1}) as observed on the (100) surface, but the activation entropy for the formation of diisopropylether is not as negative as the values observed on the (100) termination for a similar mechanism (S_N2 with antiperiplanar substitution), probably because of the particularly strongly negative adsorption entropy of the second isopropanol molecule (−213 J·K^{-1}·mol^{-1}, vs −143 J·K^{-1}·mol^{-1} for the weak adsorption modes on the (100) surface).

DOI: 10.1021/acscatal.5b00723
ACS Catal. 2015, 5, 4423−4437

Isopropanol adsorption may thus be favored on the (110) termination, but this surface is found to be less reactive toward isopropanol than the (100) termination for all dehydration pathways. Indeed, the highest intrinsic rate constant calculated for the formation of propene on the (100) and (110) terminations are respectively 5.6×10^{-2} and 2.1×10^{-4} s^{-1}, with more than 2 orders of magnitude in favor of the (100) facets. Although the same type of aluminum atom can be found on both planes, very few basic oxygen atoms are present on (110), due to surface hydroxylation. Both the abstraction of the β hydrogen atom and the abstraction of the proton from the OH group of the second isopropanol molecule (see Figure 2) require such a basic site in order to efficiently promote propene and diisopropylether formation, respectively. Steric hindrance relative to the nonplanarity of this surface compared to the dehydrated (100) terminations may also be invoked.

d. Effect of Sodium Poisoning of the (100) Surface. Sodium poisoning has been shown to strongly decrease the isopropanol dehydration rate. Several authors determined that the number of deactivated sites is about 1 order of magnitude higher than the number of sodium cations introduced.[59,60,68] They proposed that long-range inductive effects of sodium on the Lewis acidity of aluminum atoms are responsible for this behavior. In order to investigate this hypothesis, we used surface models for the (100) termination of γ-alumina containing one (Na^+, OH^-) group per unit cell, derived from previous calculations by Digne et al.[69] They showed that the sodium cation is located in a surface vacancy between the O_{3a}, $O_{3a'}$, O_4, O_{3b} oxygen atoms, and is accompanied by a OH^- group (for the sake of electroneutrality) located on the adjacent Al_{Va} aluminum atom (Figure 13). Roy et al.[37] used a small

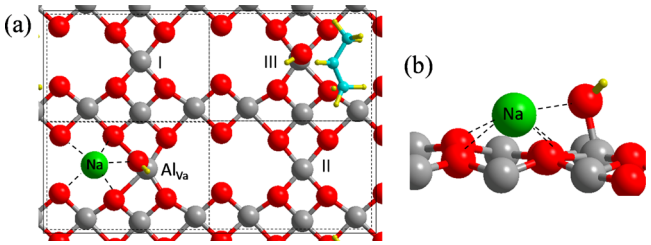

Figure 13. Activated complex of the formation of propene from isopropanol on a sodium-doped surface model for the (100) surface (green: sodium atom). (a): top view; the plain square represents the periodic simulation cell while the dotted squares figure the elementary cells of the γ-alumina surface model, one of which is here occupied by a (Na^+,OH^-) adsorbate. (b): perspective view of the (Na^+,OH^-) adsorbate. Same color code as in previous figures, with green representing Na.

cluster to describe the Na-poisoned alumina surface, with only one tricoordinated Al_{III} ion as Lewis acidic site and sodium ions added on the side of the cluster, which does not allow the detection of potential long-range effects.

NaOH and $NaNO_3$ precursors leading to similar catalytic behaviors, we will assume that the (Na^+,OH^-) adsorbed model describes the surface state after calcination for both precursors. One (Na^+,OH^-) group was added per simulation cell, occupying one Al_{Va} site and the adjacent vacancy. We considered the reactivity of the three remaining Al_{Va} sites within the simulation cell, noted I, II, and III in Figure 13. Distances between the Na^+ cation and these sites are listed in Table 6. The adsorption enthalpies of isopropanol have been calculated (Table 6). As observed on the nondoped surface, the

Table 6. Modes and Enthalpies of Adsorption of Isopropanol on the I, II, and III Al_{Va} Sites in the Presence of Coadsorbed NaOH, and Activation Parameters for the Formation of Propene through E2 Mechanism[a]

site	Na−Al distance (Å)	adsorption			reactivity	
		mode	$\Delta_{ads}H°$	$\Delta_{ads}S°$	$\Delta_rH^‡$	$\Delta_rS^‡$
I	6.0	associated	−111	−155	120	−16
II	10.9	dissociated	−119	−189	125	9
III	12.1	dissociated	−120	−192	126	+4
nondoped	-	dissociated	−121	−186	125	−8

[a]Data are calculated at 200 °C and compared with the data obtained on the non-doped surface. Corresponding activated complexes are given in the Supporting Information, Figure S20. Enthalpies are given in kJ·mol^{-1}, and entropies in J·K^{-1}·mol^{-1}.

favored adsorption mode of isopropanol involves a dissociation of its O−H bond and yields similar adsorption enthalpies (around −120 kJ·mol^{-1}) on the most distant II and III sites. However, on site I, which is the closest to the Na^+ cation, the most stable adsorption mode does not involve the dissociation of the OH bond, and the adsorption enthalpy is higher by 10 kJ·mol^{-1}.

The reaction pathways leading from the adsorbed alcohol to propene through a E2 mechanism have been calculated in the presence of coadsorbed (Na^+,OH^-). The calculated activation enthalpies and entropies (Table 6) show little difference from the values on the nondoped surface in the three cases, the activated complex presenting a very similar structure.

Thus, no long-range interactions induced by the sodium introduction are observed, and only slight modifications of the adsorption mode on the nearest site (I) can be anticipated. Note that the results in terms of adsorption and reactivity are similar if the sodium ion is replaced by a proton—in other terms, by a coadsorbed, dissociated water molecule—which indicates that the slight modifications observed here have to be attributed to the adsorbed OH^- moiety rather than to the sodium ion (see Supporting Information, Figure S19, S20 and Table S3). Nonetheless, the adsorption of (Na^+,OH^-) physically poisons one Al_{Va} site as an adsorbed water molecule would do, but this former entity is unlikely to desorb upon activation of the catalyst, while a water molecule may desorb, depending on the activation conditions.

4. DISCUSSION

4.1. Nature of the Alumina Active Face. The experimental evidence provided in this study suggests that a similar ensemble of adjacent active sites on dehydrated (100) terminations is involved in both conversion routes of isopropanol on γ-alumina and derived materials, leading to propene and diisopropylether. It was shown that, for a given isopropanol conversion at a given temperature, the selectivity of the reaction was unaffected by

- changing the activation temperature (i.e., changing the OH coverage);
- changing the structure of the support from γ- to δ-alumina (i.e., changing the proportion of (100) terminations);
- poisoning by sodium (i.e., decreasing the activity of the catalyst in all the routes involved in the dehydration process).

DOI: 10.1021/acscatal.5b00723
ACS Catal. 2015, 5, 4423−4437

In terms of facets involved, our conclusions are in agreement with those drawn by Kwak et al. regarding ethanol dehydration,[28] who also found the (100) termination to be the most reactive surface. They are also supported by our *ab initio* study. It must be emphasized that, if the (100) surface model had formerly been used for similar studies regarding ethanol dehydration,[36,38,39] the (110) surface model used here takes into account the surface reconstruction recently proposed by Wischert et al.[56] which to the best of our knowledge leads to the most stable surface and has never been considered before.

In the present paper, the extent of hydration of the (100) and (110) surfaces (dehydrated and partially hydrated, respectively) was selected on the basis of a comparison between initial reaction rates and thermodynamic considerations. In a recent paper, Christiansen et al.[41] have investigated the unique Al site of dehydrated surface (111) as a common active site for both dehydration pathways. This termination is usually considered as less abundant with respect to surfaces (100) and (110) and would be highly hydrated in our experimental conditions;[55] it was not considered here.

In all cases, isopropanol is shown to adsorb more favorably as an alcoholate on specific Lewis acidic sites. On the partially hydrated (110) surface, the key feature that would explain a lower reactivity seems to be the lack of basic species in the vicinity of the adsorbates, leading to higher activation enthalpies for both the formation of propene and of diisopropylether than on dehydrated (100). This is in contrast with former studies in which this surface was found to be more reactive than the (100) termination; however, in these cases, the (110) surface was supposed to be dehydrated,[39] which is unlikely under the reaction conditions. This emphasizes the critical role of acid−base pairs on the surface for the dehydration of alcohols, and matches previous experimental[29] or theoretical results.[40]

4.2. Nature of the Active Site and Mechanism. On the (100) surface, a specific site (Al_{Va}) has been found to be able to adsorb isopropanol, to form both propene and diisopropylether with quite low activation enthalpies (125 and 112 kJ·mol^{-1}) and to transform the ether into propene and isopropanol (118 kJ·mol^{-1}). We have shown that the proximity of the base center with the Al atom is determining, but the nature of the base center (OH group or oxygen atom) is not. Table 7 shows the comparison between calculated activation enthalpies on the (100) surface (site Al_{Va}), on the (110) surface, and experimentally measured activation enthalpies. The experimental data match the calculated values on the (100) surface quite well. In line with Christiansen et al.[38] who investigated ethanol dehydration, we support a S_N2 mechanism for the formation of the ether, although the mechanism proposed by Jain and Pilai,[31] involving a weakly adsorbed, electrophilic second alcohol molecule, is found more favorable in the present work for a secondary alcohol like isopropanol. In contradiction with previous publications (related to ethanol),[36,38] we found that $E1_{cb}$ and E2 mechanisms for propene formation, which may both explain a primary kinetic isotope effect linked to the C−H bond breaking,[23,30] are competitive from the enthalpic point of view, but we exclude the former on the basis of entropic considerations.

Table 7. Activation Parameters Calculated for the Most Favorable Pathways on the (100) and (110) Surfaces, and the Experimentally Determined Enthalpy of Activation on γ-Alumina[a]

		(100) surface	(110) surface	experimental
formation of propene	$\Delta_rH^{\ddagger}$ (kJ·mol^{-1})	125	158	128
	$\Delta_rS^{\ddagger}$ (J·K^{-1}·mol^{-1})	−8	+14	-
formation of diisopropylether	$\Delta_rH^{\ddagger}$ (kJ·mol^{-1})	112	130	118
	$\Delta_rS^{\ddagger}$ (J·K^{-1}·mol^{-1})	−36	−13	-

[a]Energies and enthalpies are given in kJ·mol^{-1}, entropies in J·K^{-1}·mol^{-1}, and are calculated at 200 °C.

It should be noted, however, that we cannot exclude the role of additional sites, such as Al_{Vc} on the (100) facets, which only promote the formation of propene, or noninvestigated defect sites (like corner or edges), which were proposed by Phung et al. as the active sites.[70]

The lower selectivity measured for diisopropylether cannot be related to the activation enthalpy—which is actually in favor of the formation of ether, both from experiments and calculations—nor to a difference in active site density, as both products can be produced on the same type of active site. We propose that an entropic factor plays a significant role in the selectivity: indeed, as shown in Table 6, the activation entropy for the formation of propene is less negative than that for the formation of ether. The calculated activation Gibbs free energy, and thus the rate constant that can be derived, lie in the same range. The weak adsorption of the second alcohol required to produce diisopropylether may also be a factor which acts in favor of the formation of propene.

4.3. Role of Water. The influence of water on dehydration reactions was shown to be decisive in many previous publications and is often considered as a poison[34] or as an inhibitor of the reaction.[15,25,71,72] Our study suggests that two effects of water can be expected:

- We have shown that alumina does not deactivate under reaction conditions despite the production—and possible adsorption—of water during the process (at least for the conversions examined in this paper). This can be understood as water adsorbs more weakly than isopropanol on the surface, as shown by DFT results, and is displaced by isopropanol from the gas-phase (provided that there is still sufficient isopropanol in the gas-phase).
- However, we also demonstrate (see Figure 5a) that the initial isopropanol dehydration rate at 200 °C is low when the activation temperature is low and the surface is highly hydroxylated. This indicates that when the density of adsorbed OH groups is initially high (activation at low temperature), isopropanol cannot displace preadsorbed water molecules. Otherwise, water would always be swept away upon isopropanol introduction and the activated surface would be identical and have the same behavior whatever their initial hydration state. In these conditions, water can behave as a poison for the catalyst.

A reason for that behavior could be that preadsorbed water forms a strong network of hydrogen bonding, and does not desorb sequentially, but by "patches" that leave a locally dehydrated surface. The higher the activation temperature, the more dehydrated zones appear on the surface, and the more active sites are accessible. For an activation temperature of 450 °C or higher, the (100) surfaces are almost entirely accessible (this is actually the thermodynamic state of the surface as we show in our calculations), hence the maximum dehydration

DOI: 10.1021/acscatal.5b00723
ACS Catal. 2015, 5, 4423−4437

activity. During reaction, adsorption competition takes place only between isopropanol molecules and individual adsorbed water molecules, that are not as strongly H-bonded as preadsorbed OH groups, which may display cooperative effects.

4.4. Role of Sodium Poisoning. Srinivasan et al.[59] observed from TPD experiments that small amounts of sodium (<2000 ppm) cause the deactivation of the most active sites, which may still react but at the cost of a higher reaction temperature. The reason behind this phenomenon is not really understood. The disappearance of acidic protons replaced by sodium atoms should not explain this feature, as we showed that Brønsted acidity is not involved in this reaction. Lavalley et al.[68] proposed that due to long-range interactions, one sodium ion is able to deactivate up to 10 active sites. Our calculations do not allow us to observe any long-range effect of the coadsorption of a (Na^+, OH^-) species in the vicinity of an active site. The conclusions of Lavalley et al. actually rely on the assumption that all Lewis acidic sites detected by pyridine adsorption are active for catalysis, while we show that some of the γ-alumina Lewis acidic sites—for example, those located on the (110) terminations—are less active toward isopropanol dehydration than others on the (100) surfaces.

We propose instead that the (OH^-) species associated with the Na^+ ion are very unlikely to desorb during activation, or to be displaced by isopropanol molecules from the gas-phase. It can be inferred that sodium ions prevent water molecules from desorbing and from liberating the active site during activation. This would explain that a low-temperature activation (and thus the presence of preadsorbed water) and Na-poisoning of the surface have the same kind of effects on the γ-alumina reactivity toward isopropanol

If we consider that the Al_{Va} sites located on the (100) terminations (20% of the total specific area) are the only active sites on γ-alumina, we can calculate a mean site density of 6.8×10^{-7} mol·m^{-2}, while the mean sodium density introduced is of 3.1×10^{-7} mol·m^{-2}. As the initial intrinsic reaction rate is decreased by 80% upon introduction of sodium, we deduce that one sodium atom poisons 1.8 active sites, which is consistent with the hypothesis that one sodium atom directly poisons one site and may alter adsorption on the nearest site. Note that Phung et al. also assessed that the number of sodium atoms and poisoned sites are of the same order of magnitude,[70] but they attributed the catalytic activity of γ-alumina to Lewis acidic sites located to the corners and edges of the particles.

5. CONCLUSION

Through a combination of detailed experimental kinetic studies and DFT calculations, we examined the alkene-to-ether selectivity issue in the isopropanol transformation into propylene and diisopropylether on the (100) and (110) surfaces of γ-alumina. Both approaches suggest that all elementary steps required to explain the reaction mechanism of isopropanol dehydration occur on a single set of active sites. This is shown by (i) tuning the amount of active sites by comparing γ and δ polymorphs, (ii) varying the activation temperature of the samples to modify the OH coverage, (iii) sodium poisoning, (iv) calculating reaction steps for the production of propene and ether on the two surface orientations at relevant hydroxyl coverage. The presence of a pentacoordinated Al_V as a Lewis acidic site and of a basic species in the vicinity are required to efficiently catalyze three elementary steps: the direct formation of propene and of diisopropylether, and the conversion of diisopropylether into propene and isopropanol. For this purpose, the (100) facets seem more suited than the (110) terminations, which lack basic enough sites because they remain partially hydrated. We also provide insight into the origin of sodium poisoning effects, observed to be a short-range effect, linked to the residual hydroxylation of most reactive sites in the neighborhood of sodium cations. As a consequence, the activity of the catalyst will be a function of the amount of (100) surface exposed, but the higher selectivity observed for propene mainly depends on the activation thermodynamic parameters: while the activation enthalpy is close for the two direct reactions, the formation of propene is entropically favored over the formation of diisopropylether. Thus, our results suggest that for the given conditions of catalytic tests, selectivities on alumina may only be tuned by changing the reaction temperature, and not by changing the morphology of the material, or its water or sodium coverage.

■ ASSOCIATED CONTENT

Supporting Information

The Supporting Information is available free of charge on the ACS Publications website at DOI: 10.1021/acscatal.5b00723.

Experimental X-ray powder diffractograms of the materials; additional computational methodology details; experimental kinetics data (Arrhenius plots, pressure evolutions); calculated evolution of the thermodynamic function along the reaction paths; additional calculated activated complexes structures (PDF)

■ AUTHOR INFORMATION

Corresponding Authors

*E-mail: kim.larmier@upmc.fr. Tel: +33 1.44.27.55.12 (K.L.).
*E-mail: celine.chizallet@ifpen.fr. Tel: +33 4.37.70.22.42 (C.C.).
*E-mail: eric.marceau@upmc.fr. Tel: +33 1.44.27.60.04 (E.M.).

Notes

The authors declare no competing financial interest.

■ ACKNOWLEDGMENTS

This work was granted access to the HPC resources of CINES and IDRIS under the allocations 2013-x2013087014 and 2014-x2014087014 made by GENCI (Grand Équipement National de Calcul Intensif). All calculations were performed at GENCI and at IFPEN HPC center ENER110. The authors acknowledge Dr Pascal Raybaud and Dr André Nicolle (IFP Energies nouvelles) for the fruitful discussions they had, and Antoine Bach for his help with kinetic measurements presented in the Supporting Information document.

■ REFERENCES

(1) Alonso, D. M.; Bond, J. Q.; Dumesic, J. A. *Green Chem.* **2010**, *12*, 1493−1513.
(2) Serrano-Ruiz, J. C.; Dumesic, J. A. *Energy Environ. Sci.* **2011**, *4*, 83−99.
(3) Zhou, C.-H.; Xia, X.; Lin, C.-X.; Tong, D.-S.; Beltramini, J. *Chem. Soc. Rev.* **2011**, *40*, 5588−5617.
(4) Lin, Y.-C.; Huber, G. W. *Energy Environ. Sci.* **2009**, *2*, 68−80.
(5) Sun, Y.; Cheng, J. *Bioresour. Technol.* **2002**, *83*, 1−11.
(6) Lee, J.; Parameswaran, B.; Lee, J.; Park, S. *J. Sci. Ind. Res. (India).* **2008**, *67*, 865−873.
(7) Dürre, P. *Appl. Microbiol. Biotechnol.* **1998**, *49*, 639−648.
(8) Jojima, T.; Inui, M.; Yukawa, H. *Appl. Microbiol. Biotechnol.* **2008**, *77*, 1219−1224.

DOI: 10.1021/acscatal.5b00723
ACS Catal. 2015, 5, 4423−4437

(9) Collas, F.; Kuit, W.; Clément, B.; Marchal, R.; López-Contreras, A. M.; Monot, F. *AMB Express* **2012**, *2*, 45−55.
(10) Ai, M. *Bull. Chem. Soc. Jpn.* **1977**, *50*, 2579−2583.
(11) Lauron-Pernot, H. *Catal. Rev.: Sci. Eng.* **2006**, *48*, 315−361.
(12) Knozinger, H.; Buhl, H.; Ress, E. *J. Catal.* **1968**, *12*, 121−128.
(13) Clayborne, P. A.; Nelson, T. C.; DeVore, T. C. *Appl. Catal., A* **2004**, *257*, 225−233.
(14) Dabbagh, H.; Mohammad Salehi, J. *J. Org. Chem.* **1998**, *63*, 7619−7627.
(15) Knozinger, H.; Köhne, R. *J. Catal.* **1966**, *5*, 264−270.
(16) Knozinger, H.; Buhl, H. *Berichte der Bunsen-Gesellschaft* **1967**, *71*, 73−77.
(17) Kallo, D.; Knozinger, H. *Chem. Ing. Tech.* **1967**, *39*, 676−680.
(18) Knozinger, H.; Ress, E. *Z. Phys. Chem.* **1967**, *54*, 136−149.
(19) Knozinger, H.; Stolz, H. *Kolloid Z. Z. Polym.* **1968**, *223*, 42−47.
(20) Knozinger, H.; Ress, E. *Z. Phys. Chem.* **1968**, *59*, 49−62.
(21) Knozinger, H.; Buhl, H. *Z. Phys. Chem.* **1969**, *63*, 199−201.
(22) Knozinger, H.; Scheglila, A. *Z. Phys. Chem.* **1969**, *63*, 197−198.
(23) Knozinger, H.; Scheglila, A. *J. Catal.* **1970**, *17*, 252−263.
(24) Knozinger, H.; Stolz, H. *Berichte der Bunsen-Gesellschaft* **1970**, *74*, 1056−1063.
(25) Moravek, V.; Kraus, M. *J. Catal.* **1984**, *87*, 452−460.
(26) Decanio, E. *J. Catal.* **1992**, *135*, 444−457.
(27) Golay, S.; Doepper, R.; Renken, A. *Appl. Catal., A* **1998**, *172*, 97−106.
(28) Kwak, J. H.; Mei, D.; Peden, C. H. F.; Rousseau, R.; Szanyi, J. *Catal. Lett.* **2011**, *141*, 649−655.
(29) Berteau, P.; Ceckiewicz, S.; Delmon, B. *Appl. Catal.* **1987**, *31*, 361−383.
(30) Shi, B.; Dabbagh, H. A.; Davis, B. H. *Top. Catal.* **2002**, *18*, 259−264.
(31) Jain, J. R.; Pillai, C. N. *J. Catal.* **1967**, *9*, 322−330.
(32) Shi, B.; Davis, B. H. *J. Catal.* **1995**, *157*, 359−367.
(33) Phung, T. K.; Lagazzo, A.; Rivero Crespo, M. Á.; Sánchez Escribano, V.; Busca, G. *J. Catal.* **2014**, *311*, 102−113.
(34) Dewilde, J. F.; Chiang, H.; Hickman, D. A.; Ho, C. R.; Bhan, A. *ACS Catal.* **2013**, *3*, 798−807.
(35) Cai, S.; Sohlberg, K. *J. Mol. Catal. A: Chem.* **2003**, *193*, 157−164.
(36) Kwak, J. H.; Rousseau, R.; Mei, D.; Peden, C. H. F.; Szanyi, J. *ChemCatChem* **2011**, *3*, 1557−1561.
(37) Roy, S.; Mpourmpakis, G.; Hong, D.; Vlachos, D. G.; Bhan, A.; Gorte, R. J. *ACS Catal.* **2012**, *2*, 1846−1853.
(38) Christiansen, M.; Mpourmpakis, G.; Vlachos, D. *ACS Catal.* **2013**, *3*, 1965−1975.
(39) Jenness, G. R.; Christiansen, M. A.; Caratzoulas, S.; Vlachos, D. G.; Gorte, R. J. *J. Phys. Chem. C* **2014**, *118*, 12899−12907.
(40) Kostestkyy, P.; Yu, J.; Gorte, R. J.; Mpourmpakis, G. *Catal. Sci. Technol.* **2014**, *4*, 3861−3869.
(41) Christiansen, M. A.; Mpourmpakis, G.; Vlachos, D. G. *J. Catal.* **2015**, *323*, 121−131.
(42) Kresse, G.; Furthmuller, J. *Phys. Rev. B: Condens. Matter Mater. Phys.* **1996**, *54*, 11169−11186.
(43) Kresse, G.; Hafner, J. *Phys. Rev. B: Condens. Matter Mater. Phys.* **1994**, *49*, 14251−14269.
(44) Perdew, J. P.; Burke, K.; Ernzerhof, M. *Phys. Rev. Lett.* **1996**, *77*, 3865−3868.
(45) Grimme, S. *J. Comput. Chem.* **2006**, *27*, 1787−1799.
(46) Kresse, G.; Joubert, D. *Phys. Rev. B: Condens. Matter Mater. Phys.* **1999**, *59*, 1758−1775.
(47) Henkelman, G.; Jonsson, H. *J. Chem. Phys.* **2000**, *113*, 9978−9985.
(48) Fleurat-Lessard, P. Opt'n Path. http://perso.ens-lyon.fr/paul.fleurat-lessard/index.html (accessed February 1, 2013).
(49) Henkelman, G.; Uberuaga, B. P.; Jónsson, H. *J. Chem. Phys.* **2000**, *113*, 9901−9904.
(50) Pulay, P. *Chem. Phys. Lett.* **1980**, *73*, 393−398.
(51) Henkelman, G.; Jónsson, H. *J. Chem. Phys.* **1999**, *111*, 7010−7022.
(52) De Moor, B. A.; Reyniers, M.-F.; Marin, G. B. *Phys. Chem. Chem. Phys.* **2009**, *11*, 2939−2958.
(53) Canduela-Rodriguez, G.; Sabbe, M. K.; Reyniers, M.-F.; Joly, J.-F.; Marin, G. B. *Phys. Chem. Chem. Phys.* **2014**, *16*, 23754−23768.
(54) Digne, M.; Sautet, P.; Raybaud, P.; Euzen, P.; Toulhoat, H. *J. Catal.* **2002**, *211*, 1−5.
(55) Digne, M.; Sautet, P.; Raybaud, P.; Euzen, P.; Toulhoat, H. *J. Catal.* **2004**, *226*, 54−68.
(56) Wischert, R.; Laurent, P.; Copéret, C.; Delbecq, F.; Sautet, P. *J. Am. Chem. Soc.* **2012**, *134*, 14430−14449.
(57) Euzen, P.; Raybaud, P.; Krokidis, X.; Toulhoat, H.; Le Loarer, J.-L.; Jolivet, J. P.; Froidefond, C. In *Handbook of Porous Materials*; Schuth, F., Sing, K. S. W., Weitkamp, J., Eds.; Wiley-VCH: Weinheim, 2002; p 1591.
(58) Narayanan, C. R.; Srinivasan, S.; Datye, A. K.; Gorte, R.; Biaglow, A. *J. Catal.* **1992**, *138*, 659−674.
(59) Srinivasan, S.; Narayanan, C. R.; Biaglow, A.; Gorte, R.; Datye, A. K. *Appl. Catal., A* **1995**, *132*, 271−287.
(60) Srinivasan, S.; Narayanan, C. R.; Datye, A. K. *Appl. Catal., A* **1995**, *132*, 289−308.
(61) Joubert, J.; Fleurat-Lessard, P.; Delbecq, F.; Sautet, P. *J. Phys. Chem. B* **2006**, *110*, 7392−7395.
(62) Joubert, J.; Salameh, A.; Krakoviack, V.; Delbecq, F.; Sautet, P.; Copéret, C.; Basset, J. M. *J. Phys. Chem. B* **2006**, *110*, 23944−23950.
(63) Carey, F. A.; Sundberg, R. J. *Advanced Organic Chemistry*, 5th ed.; Springer: New York, 2007; pp 546−557.
(64) Amatore, C.; Jutand, A. *J. Organomet. Chem.* **1999**, *576*, 254−278.
(65) Kozuch, S.; Shaik, S. *Acc. Chem. Res.* **2011**, *44*, 101−110.
(66) Rozanska, X.; van Santen, R.; Hutschka, F.; Hafner, J. *J. Am. Chem. Soc.* **2001**, *123*, 7655−7667.
(67) Leydier, F.; Chizallet, C.; Costa, D.; Raybaud, P. *J. Catal.* **2015**, *325*, 35−47.
(68) Saad, A. B. M.; Ivanov, V. A.; Lavalley, J. C.; Nortier, P.; Luck, F. *Appl. Catal., A* **1993**, *94*, 71−83.
(69) Digne, M.; Raybaud, P.; Sautet, P.; Guillaume, D.; Toulhoat, H. *Phys. Chem. Chem. Phys.* **2007**, *9*, 2577−2582.
(70) Phung, T. K.; Herrera, C.; Larrubia, M. Á.; García-Diéguez, M.; Finocchio, E.; Alemany, L. J.; Busca, G. *Appl. Catal., A* **2014**, *483*, 41−51.
(71) Knozinger, H.; Kochloefl, K.; Meye, W. *J. Catal.* **1973**, *28*, 69−75.
(72) De Mourgues, L.; Peyron, F.; Trambouze, Y.; Prettre, M. *J. Catal.* **1967**, *7*, 117−125.

DOI: 10.1021/acscatal.5b00723
ACS Catal. 2015, 5, 4423−4437